Proceedings of the XVIII ECSMGE 2024

GEOTECHNICAL ENGINEERING CHALLENGES
TO MEET CURRENT AND EMERGING NEEDS OF SOCIETY
© 2024 the Authors
ISBN 978-1-032-54816-6
DOI 10.1201/9781003431749-257
Open Access: www.taylorfrancis.com, CC BY-NC-ND 4.0 license



Back analysis of flexible barrier response following an open hillslope landslide impact at Pa Mei, Hong Kong

Analyse rétrospective de la réponse d'une barrière flexible suite à un impact de glissement de terrain sur une pente ouverte à Pa Mei, Hong Kong

E.K.L. Wong*, J.W.C. Lau

Geotechnical Engineering Office, Civil Engineering and Development Department, Hong Kong, China

J.-W. He, Z.-H. Zhou, S.L. Chan
Formerly Hong Kong Polytechnic University, Hong Kong, China
*eugeneklwong@cedd.gov.hk

ABSTRACT: An open hillslope landslide occurred above Ma Wan New Village at Pa Mei on Lantau Island, Hong Kong in October 2021, involving a total debris volume of approximately 240 m³. About half of the debris was deposited on the hillside while the rest travelled further downslope to hit the edge panels of two flexible rockfall barriers, which had a rated energy capacity of 3,000 kJ. The debris was stopped and retained by the barriers with limited observable damage to the barriers. This paper documents the back analysis of the response of the flexible barriers using the finite element program LS-DYNA. A numerical simulation was first conducted to replicate a full-scale rockfall test to calibrate the flexible rockfall barrier model. The landslide impact process was then reconstructed numerically and calibrated against field observations. The impact velocity and energy were estimated from free-field debris mobility analysis and coupled debris-barrier interaction. Using the calibrated numerical model, a hypothetical landslide debris impact event close to the energy rating of the barrier system is also investigated. Future work on the design of flexible rockfall barrier systems subjected to landslide debris impact is discussed.

RÉSUMÉ: Un glissement de terrain à pente ouverte s'est produit au-dessus du Nouveau Village de Ma Wan à Pa Mei sur l'île de Lantau, à Hong Kong, en octobre 2021, impliquant un volume total de débris d'environ 240 m³. Environ la moitié des débris ont été déposés sur le flanc de la colline, tandis que le reste s'est déplacé plus loin vers le bas de la pente pour heurter les panneaux de bord de deux barrières pare-pierres flexibles, d'une capacité énergétique nominale de 3,000 kJ. Les débris ont été arrêtés et retenus par les barrières, avec des dommages visibles limités sur les barrières. Cet article documente l'analyse rétrospective de la réponse des barrières flexibles à l'aide du programme d'éléments finis LS-DYNA. Une simulation numérique a d'abord été réalisée pour reproduire un test de chute de pierres à grande échelle afin de calibrer le modèle de barrière anti-chute flexible. Le processus d'impact du glissement de terrain a ensuite été reconstruit numériquement et calibré par rapport aux observations sur le terrain. La vitesse et l'énergie d'impact ont été estimées à partir d'une analyse de la mobilité des débris en champ libre et de l'interaction couplée débris-barrière. À l'aide du modèle numérique calibré, un événement hypothétique d'impact de débris de glissement de terrain proche de la cote énergétique du système de barrière est également étudié. Les travaux futurs sur la conception de systèmes de barrières anti-pierres flexibles soumis à l'impact des débris de glissements de terrain sont discutés.

Keywords: Flexible barrier; landslide; debris impact; back analysis; LS-DYNA.

1 BACKGROUND

An open hillslope landslide occurred above Ma Wan New Village at Pa Mei, Lantau Island in October 2021. Approximately 110 m³ of landslide debris impacted on two flexible rockfall barriers (3000 kJ model). The debris was successfully stopped and retained by the flexible barriers with limited observable damage to the barriers. This incident provided a good opportunity for studying the behaviour of rockfall barriers subjected to

impact from debris consisting primarily of granular soil.

It was estimated that the landslide occurred in the evening of 9 October 2021 (Fugro, 2022). The shallow landslide was probably rain-induced and was attributed to the development of transient elevated pore water pressures within the colluvium and completely decomposed tuff layers above the shallow bedrock. The landslide source measured approximately 20 m long by 13.5 m wide by 1.5 m deep. The failure volume at the source area was

estimated at 220 m³. The length of the landslide trail between the crown of the landslide scar and the barriers was approximately 40 m. A debris volume of 20 m³ was estimated to have been entrained along the landslide path. About a third (80 m³) of the total landslide debris was observed to have deposited upslope of flexible barrier FW-1A, of which approximately 20 m³ was retained by the south-eastern edge panel of barrier FW-1A. After impact, the maximum net elongation (outward deflection) of FW-1A was found to be about 2.3 m measured from the barrier axis (i.e. line connecting base of barrier posts) from hand-held LiDAR scanning. The residual height of the barrier net was 84% of the original minimum net height of 4.9 m. The rest of the debris (160 m³) deposited upslope of lower barrier FW-1B, of which approximately 90 m³ was retained behind the barrier net in its north-western edge panel. The maximum net elongation of FW-1B after impact measured 2.8 m from the barrier axis. The residual height of the barrier net was 78% of the original minimum net height.

2 FLEXIBLE BARRIER SYSTEM

Six separate flexible barriers totalling approximately 388 m in length, were constructed in 2012 to protect the downslope area against boulder fall and open hillslope landslide hazards originating from the natural hillside.

A general view of the flexible barriers is shown in Figure 1. The barriers hit by landslide debris, FW-1A and FW-1B, were located in a largely planar natural hillside sloping at about 30°. FW-1A comprised five net panels while FW-1B comprised four net panels. All panels were approximately 12 m wide. The steel posts in the barriers consisted of 5.5 m high HEB 200 beams. Two top longitudinal "suspension cables" suspended the principal nets in alternate spans (Figure 2). Brake elements were provided to each suspension cable in alternate spans. A third longitudinal cable, the "brake cable", ran parallel to the two suspension cables. The brake cable was provided with brake elements at the centre of each span. The arrangement of the bottom longitudinal "ground cables" followed a similar arrangement, i.e. two ground cables and one brake cable. The principal net consisted of a diagonal net made up of 10 mm diameter wire ropes arranged in a 140 mm × 140 mm square pattern. The wire ropes were 6×7 IWRC stranded ropes with breaking force of 72 kN. The energy-dissipating devices (brake elements) are mobilised through friction developed as cable loads cause the wire ropes to slip through the openings in

each brake plate, tightening and taking up the available length in the wire rope loop (Figure 2). After mobilisation, the force in each brake element stays relatively constant before the maximum elongation is reached. No major signs of movement were noted in the brake elements after the incident, although signs of abrasion in the stranded ropes to the extent of 1-2 cm were observed. A more detailed description of the components and the working mechanism of the barrier system is given in Wong and Lau (2022).



Figure 1. General view of barriers FW-1A (left) and FW-1B (right) after installation in 2012.



Figure 2. Longitudinal cables and brake elements.

3 NUMERICAL MODEL

3.1 Material models and properties

The material models used in the numerical model of the 3000 kJ flexible barrier and the main input parameters are summarised in Table 1. The steel posts were modelled as elastic-perfectly plastic beam elements. Wire ropes, including those making up the diagonal net, were modelled as elastic cables which develop no internal forces in compression or bending. A typical value of the elastic modulus for stranded wire ropes was used. For stranded wire ropes, the range of the modulus of elasticity has been given as between approximately 100 and 130 GPa (e.g. DIN, 1984; Feyrer, 2000; Boroška et al., 2014). The nominal

metallic cross sectional area was used with typical values from EN 12385-2 (BSI, 2008).

Brake elements were modelled as inelastic springs with fully specified force-elongation relationships as shown in Figure 3.

Table 1. Material models and input parameters used in numerical model.

Component and element type	LS-DYNA material model	Key input parameters	
Boulder (solid)	RIGID	$\rho = 2478 \text{ kg/m}^3$	
Landslide debris (solid)	SOIL_AND_ FOAM	$\rho = 2000 \text{ kg/m}^3$ G = 6 MPa B = 12 MPa (bulk modulus) v = 0.3 c' = 1 kPa $\phi_1' = 30^\circ$	
Posts (beam)	PLASTIC_ KINEMATIC	$\rho = 7850 \text{ kg/m}^3$ $E = 205 \text{ GPa}$ $v = 0.3$ $p_y = 235 \text{ MPa}$	
Wire ropes	CABLE_	$\rho = 7900 \text{ kg/m}^3$	
(beam)	DISCRETE_	E = 120 GPa	
Net (beam)	BEAM		
Brake elements (beam)	SPRING_ INELASTIC	See Figure 3	

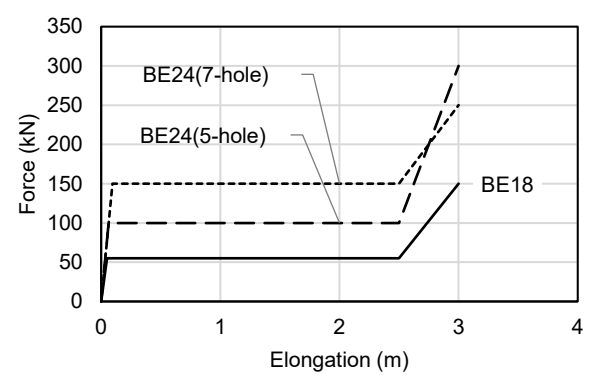


Figure 3. Force-elongation relationship of brake elements.

3.2 Replication of full-scale rockfall test

The diagonal net was tied to the suspension cables through seam ropes. It is expected that the friction between the diagonal net and suspension cables could be greater than that in ring-net type barrier nets, in which the principal net consists of ring-nets suspended from longitudinal cables directly or through shackles. Koo and Kwan (2016) carried out numerical simulation of a punching rockfall test using a coefficient of friction of μ =0.1 for the sliding contact between shackles and steel cables, with good agreement with physical test results. To model the sliding contact between the diagonal net and

suspension cables through seam ropes under the present study, different values of the coefficient of friction was attempted.

The deformed shape of the barrier is shown in Figure 4. The deceleration and location of the block was consistent between measurement and simulation results. The difference in maximum elongation of the barrier net was within 5%. The overall mode and magnitude of deformation were well reproduced in the Overall, a value of $\mu = 0.9$ returned simulation. simulation results most consistent with the physical test. The average anchorage forces for the top longitudinal cables were within about $\pm 10\%$ of the measured values in the physical test while the anchorage forces in the bottom longitudinal cables were smaller than measured values by 13%. The simulated net elongation and residual height were also within 1 to 3% of physical test results.

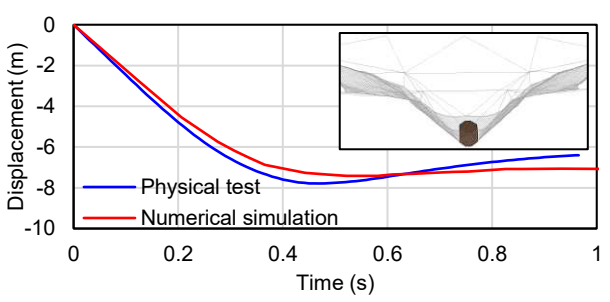


Figure 4. Displcaement of test block after impact.

3.3 Model setup for coupled analysis

The setup of the numerical model is shown in Figure 5. As-built coordinates of the barrier posts and anchorages were used to construct the numerical model. Shell elements were used to construct the threedimensional topography from airborne LiDAR data obtained in 2020 at 0.5 m resolution. Following the landslide event, hand-held LiDAR scanning of the source area was carried out. The 2020 topography was locally modified to take into account the depression at the source area resulting from the landslide. A "landslide source container" was constructed following the outline of the landslide source area delineated from field investigations. The container was topped by a "lid", which was identical to the prelandslide topography shell elements but offset vertically by a prescribed distance to make up the target landslide source volume. The landslide source was generated in the space enclosed by the container, the topography and the lid. The debris was released by lifting the landslide source container. A regular array comprising of regular tetrahedral solid elements ("the ALE mesh") was set up to define the largest possible extent of the debris.

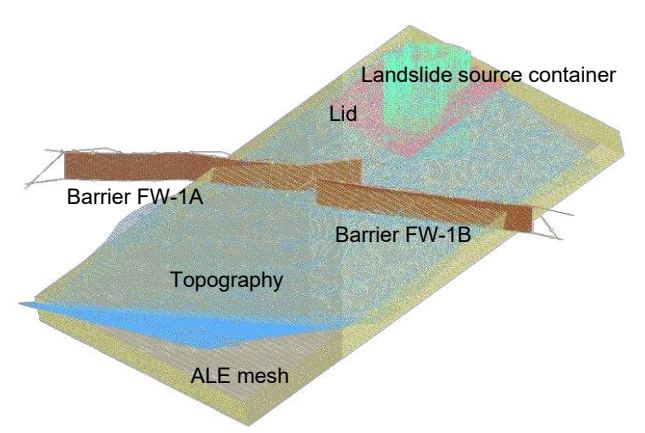


Figure 5. Numerical model setup.

Koo (2017) carried out back analysis of notable open hillslope landslides and channelised debris flows in Hong Kong using LS-DYNA. The back-calculated internal friction angle ϕ_1 of landslide debris was found to be in the range of 25° to 30° for open hillslope landslides. The back-calculated apparent basal friction angle ϕ_a was found to be 20° for the Sham Wan Road landslide (GEO and Knill, 1995), which had occurred in a similar open hillslope setting. GEO (2012) recommends that $\phi_a = 25^\circ$ and 20° should be used in mobility assessments for open hillslope landslides with source volume small than or equal to 500 m³ and larger than 500 m³, respectively.

The Drucker-Prager yield criterion was used for modelling the landslide debris (Table 1). An internal friction angle of 30° was adopted as a first estimate, while values between 27° to 32° were also attempted. The derivation of input parameters for the Drucker-Prager criterion from ϕ_i followed the procedure in Koo (2017). It is known that modelling results are not sensitive to the values of shear modulus, bulk modulus and Poisson's ratio and that sufficiently low stiffness values may be used for computational efficiency (Koo, 2017). A basal friction angle ϕ_a of 25° to 28° were attempted.

4 RESULTS OF COUPLED ANALYSIS

4.1 Barrier deformation

The frontal impact velocity, barrier deformation and debris geometry are presented in Table 2 for the case of internal friction angle of 30° and basal friction angles of 27°. The impact process is shown in Figures 6(a) and (b). The debris largely came to a stop at the end of the simulation as evidenced by the velocity contour shown in Figure 6(c). The total kinetic energy of the entire debris also reached a residual level (Figure 6(d)).

The deformation of the barriers was in general consistent with field observations (Figures 6(e) and (f)). For the upper barrier, the net elongation and the residual height were consistent with field measurements. In the simulation, a gap of about 1.5 m developed between the edge post and the net, as a result of the net elongation and sliding of the net along the longitudinal cables under the force of the oblique impact. Measurements using hand-held LiDAR scanning indicated that the opening was about 2 m wide.

4.2 Retained volume

There were uncertainties as to the relative proportions of debris depositing along the debris trail and of the debris directly retained by the barriers, given that the debris body was a continuum in the simulation. Nevertheless, the volume of debris at the upper barrier was largely consistent with field observations. Although the net elongation and the residual height of the lower barrier were also replicated reasonably well in the simulation, the debris volume was smaller than field observations. This is evidence of the challenging nature of modelling the behaviour of multiple-barrier systems, especially one involving edge impacts.

Table 2. Results of debris-barrier interaction.

	Upper barrier		Lower barrier	
	Numerical simulation	Field observation	Numerical simulation	Field observation
Debris frontal velocity at impact (m/s)	5.5	-	5.8	=
Maximum elongation of principal net (m)	2.3	2.3	2.1	2.8
Normalised residual height	82%	84%	81%	78%
Width of retained debris (m)	12	8	12	12
Volume of retained debris (m ³)	21	20	62	90

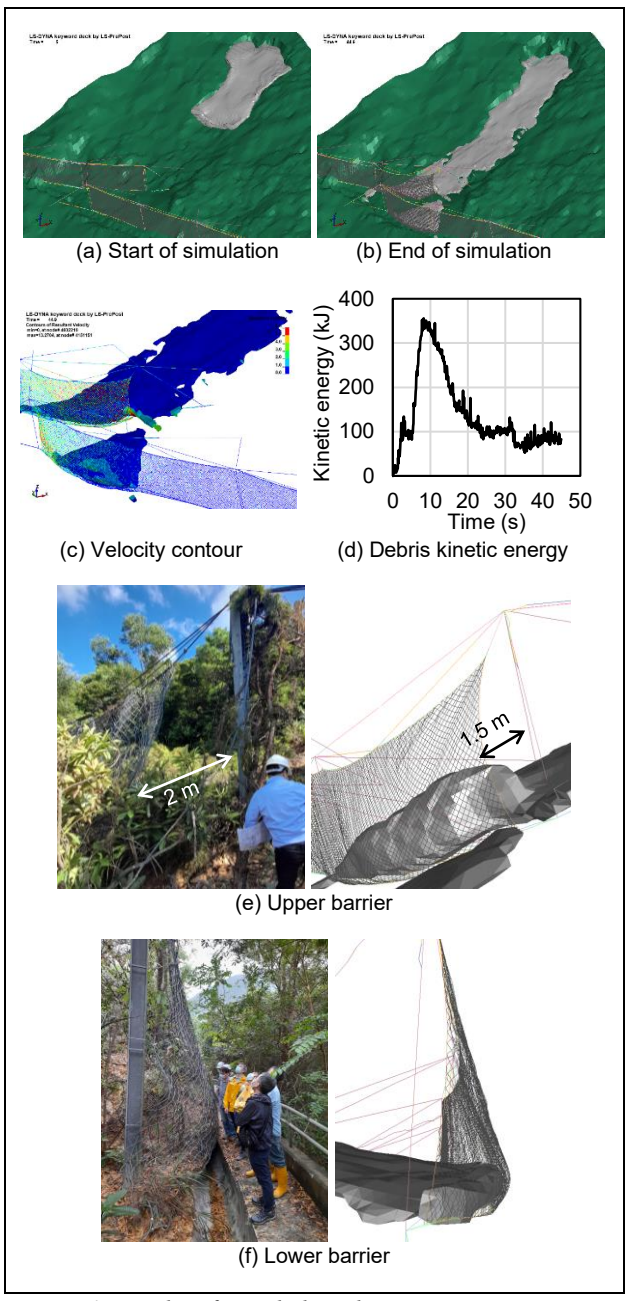


Figure 6. Results of coupled analysis.

4.3 Mobilisation of brake elements

The elongation of brake elements in the simulation was up to about 20% of the available length of the brake loops. As will be discussed later, the characteristics of the friction type brake elements make it difficult to achieve a close match between numerical and field results in terms of brake mobilisation under low energy impacts. Nevertheless, the overall deformation of the barriers was reasonably replicated in the numerical simulation. There was no overloading of wire ropes or brake elements.

4.4 Hypothetical impact scenario

Following the validation of the debris-barrier numerical model against field observations, an alternative impact scenario was studied by removing the upper barrier to investigate the condition if the lower barrier alone was subjected to a hypothetical 500 m³ event, which gives rise to an impact energy close to the energy rating of the barrier.

Without the upper barrier, the lower barrier was able to resist the 500 m³ debris impact, with greater net elongation (2.8 m) and lower residual height (77%) than either of the two barriers in the original twin-barrier layout. The brake element at the ground cable anchorage would also be mobilised to a far greater extent (30% as opposed to 17%). Nevertheless, a substantial reserve capacity was evident in terms of the utilisation of structural capacity of components and displacement limits of brake elements.

5 DISCUSSION

5.1 Impact energy

Three-dimensional debris mobility modelling using the numerical program 3d-DMM (Law et al., 2022), based on the SPH technique, was used to estimate the cumulative kinetic energy passing through the barrier locations under free-field conditions. In Hong Kong, this free-field cumulative kinetic energy is used for estimating the debris impact energy sustained by an energy-rated rockfall barrier. Although LS-DYNA could be used to perform debris mobility modelling (e.g. Koo, 2017), the computational demand is high. In this study, the frontal velocity from LS-DYNA was found to be close to 3d-DMM results, considering that the same 3D ground profile derived from LiDAR data was used in both programs. This confirms that it is reasonable to estimate the flow kinematics and impact energy using 3d-DMM.

It could therefore be estimated from 3d-DMM that the impact energy of the debris at barriers FW-1A and FW-1B was approximately 568 kJ and 421 kJ, respectively, accounting for approximately 15% to 20% of the energy capacity of the barrier. The relatively low impact energy resulted in relatively small deformations (i.e. high residual height).

Results of the present study indicate that a single barrier installed at Pa Mei would be able to resist an open hillslope landslide with a source volume of 500 m³. Results from 3d-DMM give an impact energy of about 3100 kJ, i.e. close to the energy rating of the barrier. The barrier was able to sustain the impact without overloading of structural components or excessive deformation of brake elements.

5.2 Dynamic characteristics of brake elements

For brake elements which dissipate energy by plastic deformation, studies have shown that the forces developed and hence the amount of energy dissipated are marginally greater under dynamic condition than under static condition (Lam and Sze, 2021).

The behaviour for friction type brake elements used at the Pa Mei flexible barriers appears to be different. The mobilised forces in the brake elements are consistently lower under dynamic loading. This is consistent with the general rule that static friction is greater than dynamic friction. The use of force-elongation relationships obtained from static load tests may therefore overestimate the energy dissipation capacity of a friction type brake element. Nevertheless, landslide debris generally travels at a much lower velocity than a rockfall impact with the same kinetic energy. The use of static relationships is generally considered acceptable.

6 CONCLUSION AND FUTURE WORK

The response of the flexible barriers affected by the open hillslope landslide at Pa Pei has been back analysed using LS-DYNA. The numerical model was able to reproduce the barrier deformation and debris distribution to a reasonable extent.

This back analysis has enabled the development and validation of a coupled numerical model to investigate debris-barrier interaction. It has been demonstrated that the barrier system would be able to sustain a hypothetical impact event at or above its rated energy capacity.

The validated numerical model of flexible barriers and terrain under this study would enable a supplementary study on the assessment of the energy capacity of flexible rockfall barriers subjected to landslide debris impacts. This would also allow further optimisation of the design of flexible debris-resisting barriers by fully utilising the rated energy capacity of flexible rockfall barriers and by providing guidance on the appropriate residual height to be adopted for the assessment of retention capacity.

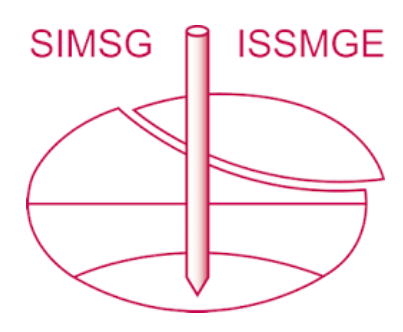
ACKNOWLEDGEMENTS

This paper is published with the permission of the Head of the Geotechnical Engineering Office and the Director of Civil Engineering and Development, the Government of the Hong Kong Special Administrative Region, China.

REFERENCES

- Boroška, J., Pauliková, A. and Ivančo, V. (2014). Determination of Elastic Modulus of Steel Wire Ropes for Computer Simulation. *Applied Mechanics and Materials*, 683, pp. 22-27, https://doi.org/10.4028/www.scientific.net/AMM.683.2 2.
- BSI (2008). BS EN 12385 2:2002+A1:2008 Steel Wire Ropes Safety Part 2: Definition, Designation and Classification. British Standards Institute, UK.
- DIN (1984). DIN 15018-1 Cranes Steel structures verification and analysis. Deutsches Institut Fur Normung, Germany.
- Feyrer, K. (2000). *Drahtseile Bemessung, Betrieb, Sicherheit* (2nd Ed.). Springer Vieweg Berlin, Heidelberg, Germany. https://doi.org/10.1007/978-3-642-54296-1.
- Fugro (2022). Detailed Study of the October 2021 Landslide on the Natural Hillside above Ma Wan New Village, Pa Mei, Tung Chung. Geotechnical Engineering Office, Hong Kong, Landslide Study Report No. LSR 2/2022.
- GEO and Knill, J. (1995). Report on the Shum Wan Road Landslide of 13 August 1995. Geotechnical Engineering Office, Hong Kong.
- GEO (2012). Guidelines on Assessment of Debris Mobility for Open Hillslope Failures. Geotechnical Engineering Office, Hong Kong, GEO Technical Guidance Note No. 34.
- Koo, R.C.H. and Kwan, J.S.H. (2016). A Numerical Study of Dynamic Responses of Two Selected Flexible Rockfall Barriers Subject to Punching and Areal Loads. Geotechnical Engineering Office, Hong Kong, GEO Report No. 323.
- Koo, R.C.H. (2017). 3D Debris Mobility Assessment Using LS-DYNA. Geotechnical Engineering Office, Hong Kong, GEO Report No. 325.
- Lam, H.W.K. and Sze, E.H.Y. (2021). Pilot Experimental Study on Brake Elements at High Strain Rate. Geotechnical Engineering Office, Hong Kong, GEO Discussion Note No. DN 2/2021.
- Law, R.P.H., Kwan, J.S.H. and Ko, F.W.Y. (2022). Validation of Geotechnical Computer Program "3d-DMM (SPH Version 2.0)". Geotechnical Engineering Office, Hong Kong, GEO Report No. 353.
- Wong, E.K.L. and Lau, J.W.C. (2022). Back Analysis of Flexible Barrier Response following Impact from the October 2021 Open Hillslope Landslide at Pa Mei, Lantau Island. Geotechnical Engineering Office, Hong Kong, Special Project Report No. SPR 3/2022.

INTERNATIONAL SOCIETY FOR SOIL MECHANICS AND GEOTECHNICAL ENGINEERING



This paper was downloaded from the Online Library of the International Society for Soil Mechanics and Geotechnical Engineering (ISSMGE). The library is available here:

https://www.issmge.org/publications/online-library

This is an open-access database that archives thousands of papers published under the Auspices of the ISSMGE and maintained by the Innovation and Development Committee of ISSMGE.

The paper was published in the proceedings of the 18th European Conference on Soil Mechanics and Geotechnical Engineering and was edited by Nuno Guerra. The conference was held from August 26th to August 30th 2024 in Lisbon, Portugal.